Ceramics International 46 (2020) 8615–8624

Contents lists available at ScienceDirect

Ceramics International

journal homepage: www.elsevier.com/locate/ceramint

Nonaqueous synthesis of TiO_2 nanorods using inductively coupled plasma

Hanxia Liu[1], Yongjie Zhang[1], Rong Yi, Rulin Li, Hui Deng*

Department of Mechanical and Energy Engineering, Southern University of Science and Technology. No. 1088, Xueyuan Road, Shenzhen, Guangdong, 518055, China

ARTICLE INFO

Keywords:
TiO_2 nanorods
Inductively coupled plasma
Thermal oxidation
Optical property
Hydrophilicity

ABSTRACT

Titanium dioxide (TiO_2) nanorods are widely used in many fields such as self-cleaning surfaces, photocatalytic lithography and pollutant control, owing to their outstanding physical, chemical and optical properties. Traditional methods for synthesizing TiO_2 nanorods are mostly tedious with high cost and tremendous energy consumption. In this work, TiO_2 nanorods with excellent optical, electrochemical, and hydrophilic properties were rapidly synthesized on titanium alloy (TC4) by using inductively coupled plasma (ICP) with strong chemical reactivity and high temperature characteristic. XRD patterns and SEM images confirm the conversion of TC4 into rutile TiO_2 nanorods after irradiated by ICP at 800 W for only one pass, and the nanorods tend to grow longitudinally under prolonged ICP processing. Moreover, the well-developed single-crystalline feature of TiO_2 nanorod is affirmed by TEM test. To reveal the growth mechanism of TiO_2 nanorods, three types of substrates (polished TC4 by electrochemical polishing (ECP), polished TA2 by ECP and oxidized TC4 by anodizing) were used to grow TiO_2 nanorods. However, TiO_2 nanorods with good morphology were only formed on the first type of substrate due to the existence of β phase Ti, which could suppress thermal transmission between grains. In addition, the results of UV–Vis absorption spectrum, electrochemical test, and static water contact angle of the treated TC4 samples show that TiO_2 nanorods synthesized by ICP possess excellent optical, electrochemical, and hydrophilic properties.

1. Introduction

Titanium dioxide (TiO_2) is a multifunctional ceramic material, seeking the attention of researchers because of its chemical stability, non-toxicity and superior photocatalytic activity [1,2]. In addition, TiO_2 being a wide band gap (3.0–3.2 eV) semiconductor material has been used in various fields such as photolysis of water for hydrogen production [3], dye-sensitized solar cell [4], photocatalytic degradation of pollutants [5], gas-sensitive sensors [6], electrodes for electrochemical characterization [7] and so forth. As often described, there are three types of TiO_2 crystal structure: rutile, anatase and brookite [8]. Among them, brookite is an unstable phase of TiO_2, thus only a few researches have been reported on it. Besides, rutile is a stable phase of TiO_2 at high temperature (> 400 °C) with better performance in terms of chemical stability and higher refractive index than anatase TiO_2, which is stable at relatively low temperature [9]. As compared with bulk TiO_2 with flat surface, TiO_2 with nano-ordered structure is preferred by researchers because of its unique properties such as photocatalysis and wetting property [10,11]. Till now, different array structures have been reported such as nanorods [2,4], nanobelts [12], nanowires [13] and nanotubes [14], where each type of nanostructures significantly affect their properties and consequently the applications. It has also been demonstrated that the ordered nanostructured TiO_2 arrays can effectively improve their optical properties and photocatalytic activities [15].

Recently different approaches, for instance, sol-gel method, oxidation method, hydrothermal method, chemical vapor deposition (CVD) and magnetron sputtering, have been used to synthesize various TiO_2 nanostructures [1,2]. Based on sol-gel method, Xu et al. [13] successfully obtained radially aligned TiO_2 nanowires and single crystal rutile phase nanorods together with some unchanged titanate nanobelts on polyester fabrics. Owing to uniquely mixed one-dimensional (1D) nanostructures, phase junctions, abundant surface hydroxyl groups and narrowed band gap, polyester fabrics exhibited excellent photocatalytic and antibacterial performances. Peng and Chen [11] prepared the highly dense and well-aligned rutile phase TiO_2 nanorods on the titanium substrate by thermal oxidation with acetone as the oxygen source, and the measurement of water contact angle on the TiO_2 film declared it a highly hydrophilic surface. Kim et al. [4] reported a highly efficient solar cell based on submicron (~ 0.6 μm) rutile TiO_2 nanorods synthesized by hydrothermal method, and discovered that the length of rutile nanorods, on which photovoltaic performance was markedly

* Corresponding author.
E-mail address: dengh@sustech.edu.cn (H. Deng).
[1] These two authors contributed equally to this paper.

https://doi.org/10.1016/j.ceramint.2019.12.093
Received 3 September 2019; Received in revised form 15 November 2019; Accepted 9 December 2019
Available online 13 December 2019

dependent, varied with the reaction time. Wen et al. [16] adopted the room temperature alkaline-free wet chemistry strategy and synthesized ultrathin nanobelts of anatase TiO_2, which could be used for lithium storage. Taking $Ti(O\text{-}i\text{-}Pr)_2(thd)_2$ as the growth solid precursor and the mixture $He–N_2$ as the working gas, Kment et al. [17] obtained anatase phase TiO_2 thin films by CVD. Although a variety of nanostructured TiO_2 have been synthesized using traditional methods, however, these methods are not only tedious with high cost and tremendous energy consumption but also difficult to scale up. Therefore, the development of a simple, economical and environment friendly method for the synthesis of nanostructured TiO_2 is strongly desired.

Herein, we proposed a nonaqueous method to synthesize TiO_2 nanorods by using inductively coupled plasma (ICP). It has been demonstrated that atmospheric pressure ICP can achieve not only high radical density (10^{13}–10^{17} cm^{-3}) but also high temperature (5000–7000 K) [18]. In our approach, strong chemical reactivity of ICP oxidized titanium alloy to form TiO_2 nanofilm, while high-temperature characteristic of the discharge crystallized TiO_2 nanofilm to grow nanorods. Compared with the previously stated traditional approaches, our method has three distinct advantages; (i) it is a nonaqueous process eliminating solutions as well as gaseous precursors; (ii) one-step synthesis from titanium alloy to TiO_2 nanorods makes it very simple approach; and (iii) due to the atmospheric operation, it is feasible to prepare TiO_2 nanorods on a large scale. In addition, we have also investigated the growth mechanism of TiO_2 nanorods on Ti–6Al–4V titanium alloy substrate by ICP irradiation and evaluated the optical, electrochemical, and hydrophilic properties.

2. Experimental details

2.1. Materials

Commercially available Ti–6Al–4V titanium alloy (TC4) and pure titanium (TA2, purity ≥ 99.85%) were used in this study. All the samples were sliced into a disc shape with a diameter of 15.0 mm and a thickness of 3.0 mm, and then lapped with sandpapers (from No. 400 to No. 1000) to smooth and flatten their surfaces. Before ICP treatment, all samples were rinsed with 75% alcohol by ultrasonic cleaning and finally dried with nitrogen gas. The TC4 and TA2 samples after these processes are defined as the as-received TC4 and TA2 samples respectively in this study. Electrochemical polishing (ECP) and anodizing were conducted to obtain samples with different surface morphologies and compositions in order to investigate the growth mechanism of TiO_2 nanorods using ICP. For ECP, 10 wt% methanol-based sulfuric acid (H_2SO_4) was used as the electrolyte and the lapped sample was polished at 30 V for 60 s. For anodization, 1 wt% water-based sodium hydroxide (NaOH) solution was taken as the electrolyte and lapped sample was anodized at 60 V for 60 s.

2.2. Setup of ICP

Fig. 1(a) shows the schematic of ICP equipment used in this study. The ICP torch fabricated by quartz (d_{in} = 14.2 mm and d_{out} = 16.0 mm) and the copper inductive coil wrapped around were mounted on a three-dimensional precision translational stage. Argon with flow rate of 1.5 SLM (standard liter per minute) and oxygen with flow rate of 20.0 SCCM (standard cubic centimeter per minute) were used as the supporting and the reaction gas of plasma, respectively, and the cooling gas was also argon with flow rate of 13.0 SLM. The distance between the outlet of the ICP torch and the surface of the sample was 30.0 mm. Fig. 1(b) shows a live moment in the experiment, in which the sample shown in Fig. 1(d) would move along the path depicted in Fig. 1(c) at a speed of 200 mm/min. After ICP irradiation, the surface of the sample was uniformly modified.

2.3. Characterizations

During ICP treatment, optical emission spectrometer (Ocean Optics USB4000) with the resolution of 0.2 nm was used to record the emission of ICP in the range of 200 to 1000 nm, and an infrared imager (FLIR T660) was utilized to measure the temperature of the TC4 surface. For the different crystal phases of TiO_2, X-ray diffraction (XRD, Rigaku Smartlab) was conducted to detect the as-received and treated TC4 samples, respectively. The radiation source used was CuKα, and the scan range was set to 10–80° with a step angle of 0.02°. Consequently, the phases from the XRD patterns were identified, compared with standard JCPDS database. Moreover, the surface morphology of all the samples was characterized by a field emission scanning electron microscope (FE-SEM, ZEISS Merlin) and an atomic force microscope (AFM, Bruker Dimension Edge) operating in tapping mode, and the crystal structure of the treated TC4 was studied using a transmission electron microscope (TEM, FEI F30) under 300 kV.

2.4. Performance tests

To evaluate the performance of the synthesized TiO_2 nanorods, their optical absorption, electrochemical, and hydrophilic properties were studied respectively. The UV–Vis diffuse reflectance spectra (UV–Vis DRS) of the treated samples were recorded by a spectrometer (PerkinElmer, Lambda 750s) equipped with an integrating sphere device to detect solid samples. The scanning range was set to 200–800 nm, and the scanning speed was 266.75 nm/min. All electrochemical measurements were investigated by an electrochemical workstation (CHI660E, Shanghai). A standard three-electrode system, with the sample as the working electrode, saturated Ag/AgCl as the reference electrode, and platinum foil (2 × 2 cm^2) as the counter electrode, was adopted. A 1.0 M NaOH water solution was considered as the electrolyte. The hydrophilicity of the as-received and treated TC4 samples was evaluated using a contact angle instrument (KRÜSS DSA25E). Specially, 1 μL volume of deionized water droplets were dropped at 5 different positions on the surface of each sample to conduct measurements, and the mean value and variance of water contact angle were calculated from the acquired data.

3. Results and discussion

3.1. ICP diagnostics and temperature characterization

As described in Section 1, ICP can not only oxidize TC4 to TiO_2 nanofilm but also crystallize TiO_2 nanofilm to TiO_2 nanorods owing to its strong chemical reactivity and high temperature in theory. Thus, in order to confirm the chemical reactivity, the optical emission spectroscopy (OES) of ICP was measured. OES can determine the nature of species and quantify the concentrations of active particles in ICP. The typical emission spectrum of ICP with power input of 800 W (P_{in} = 800 W), which was recorded at 30 mm from the ICP torch outlet, is shown in Fig. 2(a). It is clearly seen that the major excited species in ICP are atomic oxygen (777 and 844 nm) and argon (750, 811 and 912 nm) [19]. The atomic oxygen mainly generated by the collision of energetic electrons with oxygen atoms/molecules ($e + O \rightarrow O^* + e$, $e + O_2 \rightarrow O^* + O + e$) leads to the high oxidation potential of ICP. Therefore, using ICP to oxidize TC4 is practically feasible. Furthermore, some nitrogen peaks resulting from the ambient air during ICP operation can also be observed in the emission spectrum [20].

Fig. 2(b) indicates that the temperature of the sample surface would rise almost linearly with the increasing P_{in} of ICP. Generally, TC4 consists of α and β phase Ti, where α phase Ti can spontaneously convert to β phase Ti under the condition of high temperature. As for TiO_2, once the temperature reaches about 160 °C, TC4 are oxidized to TiO_2. And anatase phase TiO_2 would transform into rutile phase TiO_2 at high temperature (400–800 °C) [21]. At P_{in} = 300 W, the temperature of the

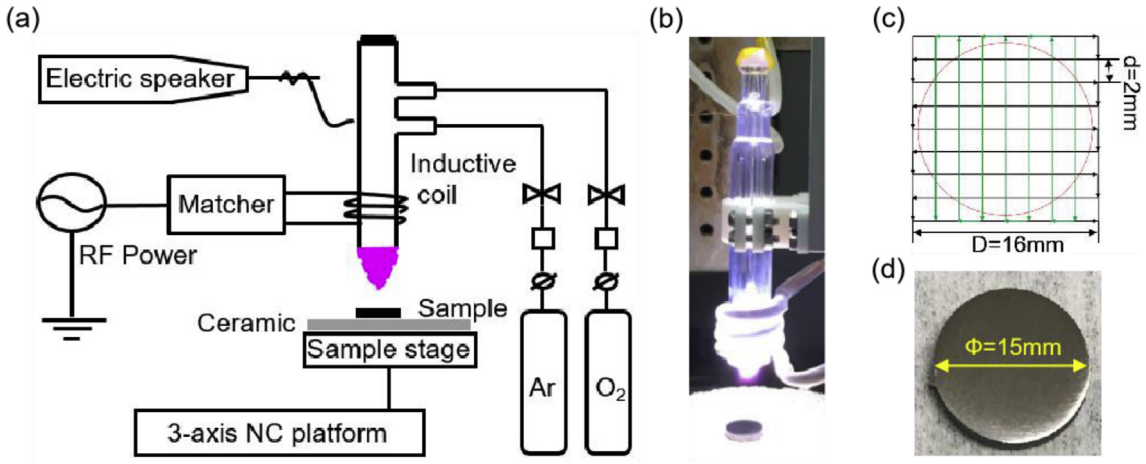

Fig. 1. (a) Schematic diagram of the ICP equipment. (b) Snapshot of the ICP treatment experiment. (c) Displacement path of the sample. (d) Photograph of the as-received TC4 sample.

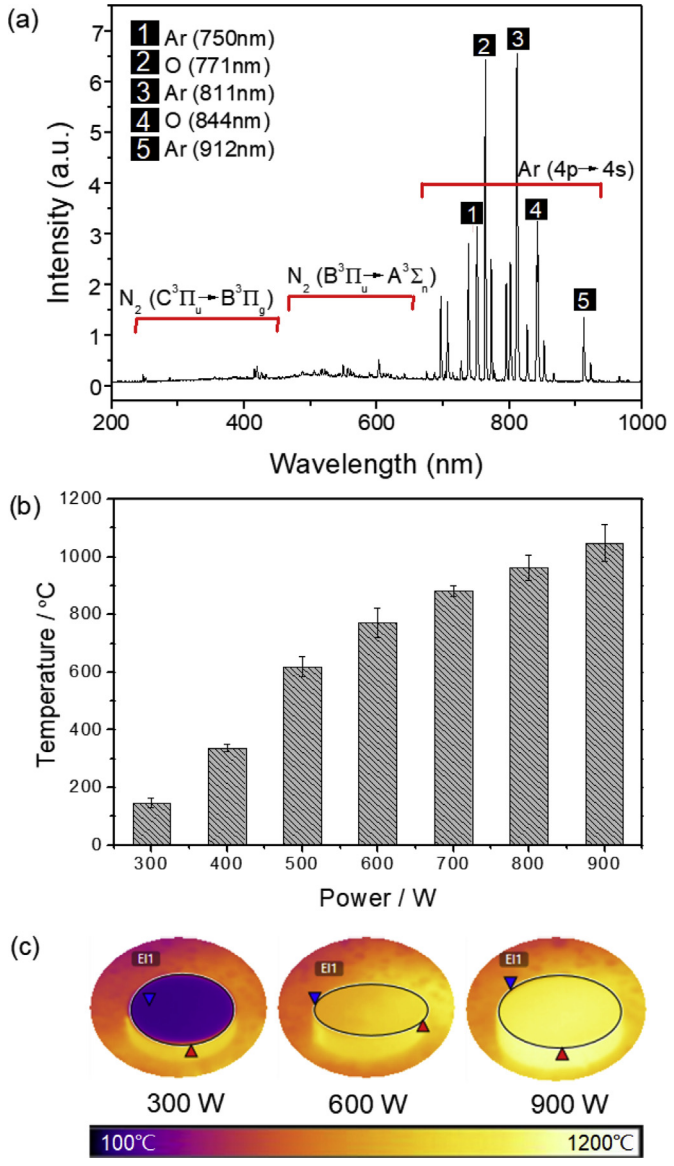

Fig. 2. (a) OES of ICP at P_{in} = 800 W. (b) Relation between the ICP power input and the temperature of the TC4 surface. (c) Temperature calibration of the TC4 surface treated by ICP at 300, 600 and 900 W.

sample surface was below 200 °C and the oxidation degree of TC4 was relatively weak. When the P_{in} increased to 500 W, the corresponding temperature raised to 600 °C, which was favorable for the formation of rutile phase TiO_2. While P_{in} = 800 W (~1000 °C) or P_{in} = 900 W (~1050 °C), TC4 surface would be oxidized deeply due to the extremely elevated temperature. Fig. 2(c) shows the temperature calibration for the treated TC4 samples by ICP irradiation at P_{in} = 300, 600, and 900 W. As the atom binding force of titanium-oxygen is greater than that of aluminum-oxygen and vanadium-oxygen [22], the titanium atoms would preferentially react with oxygen atoms to form TiO_2. However, it should be considered that the TiO_2 film might crack and even peel off because of the intense oxidation at high P_{in}.

3.2. Identification of TiO_2 phase and study of the growth conditions of TiO_2 nanorods

The common crystal structures of TiO_2 are rutile and anatase phase, while high temperature conditions are more favorable for the formation of rutile phase. XRD patterns of the as-received TC4 and the treated TC4 by ICP irradiation at different conditions are shown in Fig. 3. For the as-received TC4, typical diffraction peaks for Ti were observed, which was the same with the sample processed by ICP at P_{in} = 500 W for only one pass. However, when the P_{in} increased to 800 W, XRD peaks of rutile

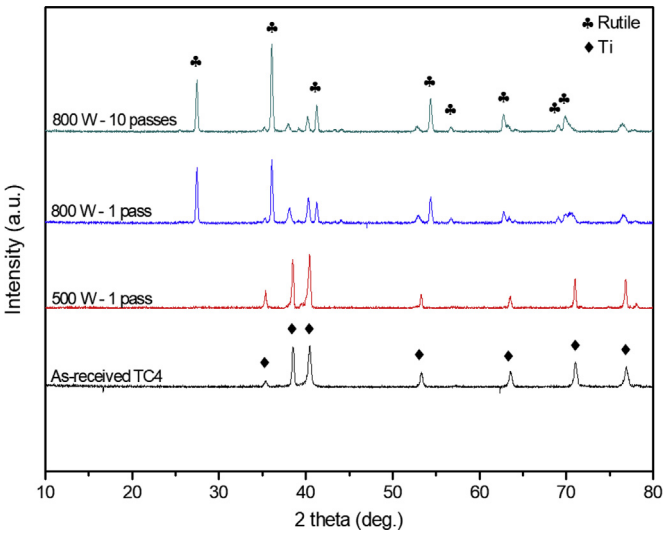

Fig. 3. Comparison of the XRD patterns of as-received and treated TC4 with the standard rutile card of JCPDS 21–1276.

were detected even for the one pass irradiation by ICP, as identified by comparing with the standard rutile card of JCPDS 21–1276. In addition, the existing diffraction peaks became sharper and their intensities got stronger due to the prolongated ICP processing time to ten passes, which reveals the constant crystal form and the continuously strengthening crystallinity of treated TC4 samples. Moreover, the average crystallite size (L) of TiO_2 based on the XRD pattern was estimated by the Scherrer formula [23]:

$$L = \frac{K\lambda}{\beta \cos\theta},$$

where K is a constant related to crystallite shape (generally taken as 0.9); λ is the wavelength of X-ray; β is the half-height width of the diffraction peak; and θ is the diffraction angle. Thus, the crystallite size of rutile on TC4 substrate irradiated at 800 W for one pass was estimated to be 40 nm. In conclusion, rutile can grow on TC4 substrate after being irradiated by ICP at enough high P_{in} even for a short reaction time, and longer reaction time contributes better crystal quality.

Actually, the high concentration of active atomic oxygens in ICP is responsible for the synthesis of rutile TiO_2 nanofilm on TC4 substrate, as explained by the following reaction pathway [24]:

$$Ti + O_2 \rightarrow TiO_2 \ \Delta G = -181.5 \text{ kcal/mol}$$

When the temperature rises to an appropriate level, TiO_2 nanofilm would crystallize to form TiO_2 nanorods. As shown in Fig. 4, the surface morphology of TC4 samples changed in different degrees after the irradiation using ICP at different P_{in}. Scratches could be observed on the control sample (Fig. 4(a)), and the oxidation of TC4 only occurred around these scratches when the P_{in} varied from 300 W to 500 W (Fig. 4(b)–4(d)). However, at higher P_{in} (600–700 W), both the temperature and chemical reactivity of ICP were enhanced, consequently oxidizing whole surface of TC4 to TiO_2. Notably, TiO_2 evenly covered the sample surface in the form of nanoparticles at first under that condition, while these TiO_2 nanoparticles grew bigger at P_{in} = 800 W and TiO_2 nanorods were formed preliminarily at P_{in} = 900 W. Concretely speaking, the lengths of TiO_2 nanorods are around 500 nm and their diameters change from 10 to 100 nm at P_{in} = 800 W, which are consistent with the values estimated by the Scherrer formula. At P_{in} = 900 W, thicker nanorods were synthesized. Thus, it seems that the improved temperature is beneficial to the transverse growth of TiO_2 nanorods.

Besides, more details of the sample surface can be recognized from the inserted AFM images. However, at $P_{in} \geq 700$ W, the surface of samples is too rough to be measured by AFM, and thus no corresponding AFM images are provided here. Fig. 4(i) shows the change in color of sample (a) to sample (h). Essentially, pure TiO_2 should be white, however varying atomic ratio of titanium and oxygen during the experiment may tune different colors of the sample [25]. In this study, the color of sample surface changed from faint yellow to dark blue and eventually turned black with the increasing P_{in} of ICP, which also depends on the increase of thickness of the TiO_2 nanofilm.

From Figs. 3 and 4, it can be concluded that ICP at high P_{in} can be used to synthesize rutile TiO_2 nanorods on the surface of TC4 substrate. Moreover, increasing P_{in} enhances the sample surface temperature; consequently, nanorods tend to grow faster in transverse direction. Thus, the transverse growth of TiO_2 nanorods is mainly determined by temperature. However, only rising temperature is not enough to obtain nanorods with good morphological characteristics.

To further reveal the growth process of TiO_2 nanorods on TC4 substrate using ICP, we firstly irradiated the stationary TC4 samples for different time at P_{in} = 800 W. Fig. 5 shows that after being irradiated for a short time (< 30s), countless TiO_2 nanoparticles grew evenly on

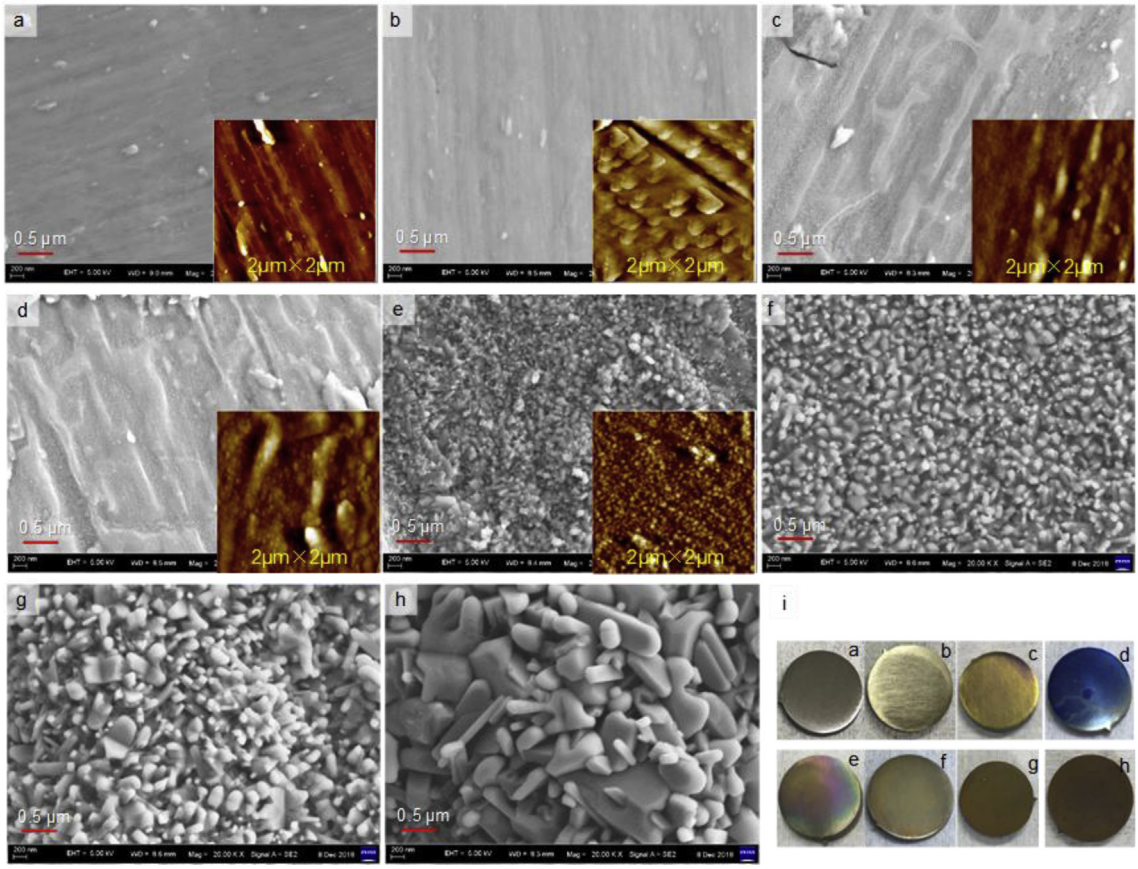

Fig. 4. Images of as-received TC4 and treated TC4 by ICP at different P_{in} for one pass. (a) As-received TC4. Treated TC4 at 300 W (b), 400 W (c), 500 W (d), 600 W (e), 700 W (f), 800 W (g) and 900 W (h). (i) Photograph of the sample (a)–(h). The insets in (a)–(e) are the corresponding AFM images.

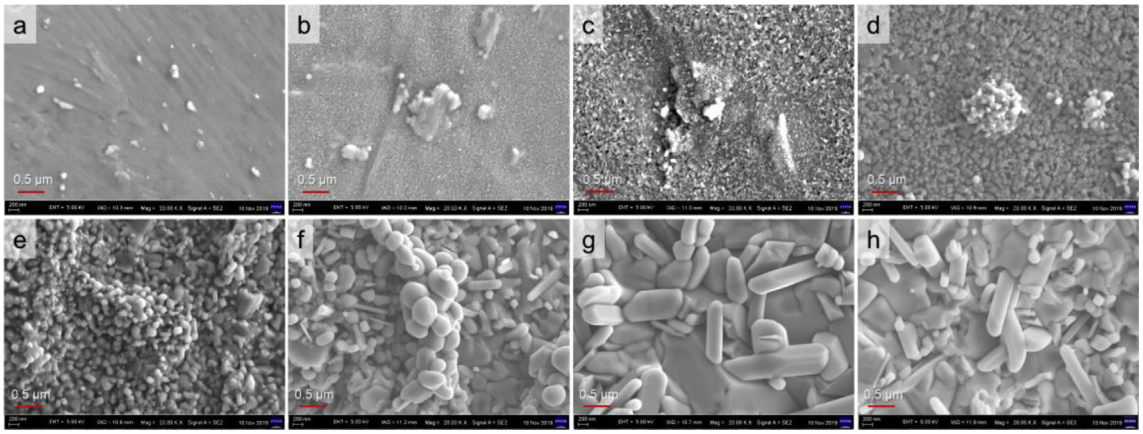

Fig. 5. SEM images of the growth trend of TiO_2 nanorod at 800 W. (a)–(h) show the morphologies of TC4 samples irradiated by ICP for 5s, 10s, 15s, 20s, 30s, 40s, 50s, 60s, respectively.

TC4 surface at first; with the extension of reaction time, these nanoparticles evolved into nanorods eventually. According to the results shown in Figs. 4 and 5, it seems that TiO_2 nanorods with good morphology are more likely to be synthesized directly and rapidly on TC4 substrate by ICP under the condition of P_{in} = 800 W.

By increasing the number of pass that plasma swept over TC4 substrate at P_{in} = 800 W, we successfully prepared lathy TiO_2 nanorods. As shown in Fig. 6, the size of the nanorods along the longitudinal direction has obviously increased under multiple irradiation passes of plasma, compared with the result of one pass in Fig. 4(g). When the plasma flame swept over the surface of TC4, TiO_2 nanoparticles grew rapidly at the site of spontaneous nucleation. With enhanced plasma processing time, TiO_2 nanoparticles self-assembled to rod-like structures. It has reported that the most stable face with the lowest surface energy would dominates the shape of TiO_2 nanorods, while the crystal face with the highest surface energy may not exist in the equilibrium shape at all [26]. Besides, these one-dimensional nanorods always tend to come together to form spheres or arrays by sharing the low surface energy crystal face in order to maintain less overall free energy [27]. At the same time, high temperature and phase transformation could lead to twins, thus forming uniform rutile TiO_2 branch-like nanostructures [24].

TEM test was completed to further study the crystal structure of TiO_2 grown by ICP irradiation. Fig. 7(a) shows a cross-sectional view of the sample in Fig. 4(c). It is clearly seen that a layer of TiO_2 with a thickness of about 20 nm was formed on the TC4 substrate only irradiated by ICP for one pass at P_{in} = 400 W. High resolution TEM (HRTEM) image in Fig. 7(b) indicates that the oxide layer was made up of polycrystalline TiO_2. The selected-area electron diffraction (SAED) pattern in Fig. 7(c) was recorded in a square area with side length greater than 100 nm, in which the boundary between TiO_2 layer and the substrate was included. Because the TiO_2 layer is too thin, Fig. 7(c) mainly represents the crystal structure of TC4. A TiO_2 nanorod with the length of about 650 nm and the width of 200 nm, which was formed under the condition of P_{in} = 800 W and five passes, is presented in Fig. 7(d). The corresponding HRTEM image (Fig. 7(e)) illustrates that the TiO_2 nanorod is well-crystallized, and clear spacings of 0.250 and 0.227 nm agree with the (101) and (111) spacing of rutile phase respectively. Additionally, the accordingly well-developed single-crystalline in nature is also displayed in Fig. 7(f).

3.3. Growth mechanism of TiO_2 nanorods

To further explore the growth mechanism of TiO_2 nanorods, we have studied the growth status of nanorods on the surface of the following three types of substrate under the conditions of P_{in} = 800 W and one pass: (i) polished TC4 sample by ECP; (ii) polished TA2 sample by ECP; and (iii) oxidized TC4 sample by anodizing.

After ECP was carried out under the corresponding parameters described in Section 2.1., two-phase structure (α and β phase) was obtained on the surface of TC4, as shown in Fig. 8(a) and (a-1). The β phase plays an important role in the formation of TiO_2 nanorods by inhibiting thermal transmission between grains during the surface treatment by ICP at P_{in} = 800 W. Hence, every grain in α phase would stay in a high temperature state, which is beneficial for the growth of TiO_2 nanorods. What's more, the growth directions of TiO_2 nanorods are unlike for different grains in α phase, as shown in Fig. 8(b) and (b-1).

For the as-received TA2 sample, scratches are obvious after lapping, as shown in Fig. 9(a), while apparent crystal boundaries can be observed on its surface after ECP, as shown in Fig. 9(b). The ECP parameters were also described in Section 2.1. Since β phase occupies only a very small proportion in TA2, it can be inferred that no β phase among these large-sized grains is present to suppress thermal transmission. Therefore, all single grains observed in Fig. 9(b) actually stay in a relatively low temperature condition when irradiated by ICP. Fig. 9(c) and (c-1) show that although nano-bulges grew on the periphery of grains, no characteristic nanorods were synthesized.

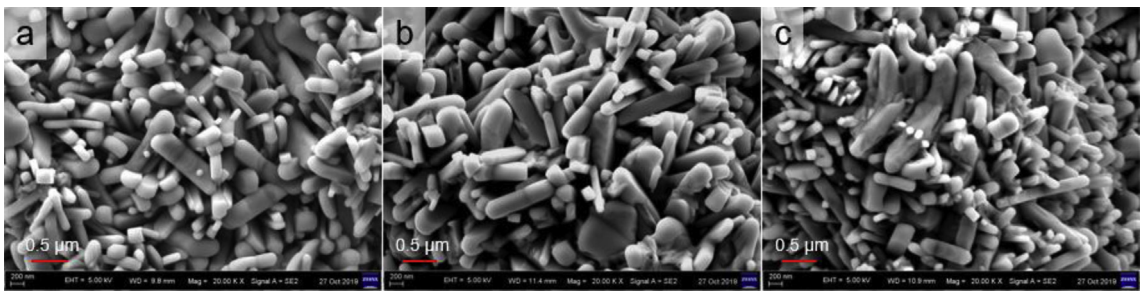

Fig. 6. SEM image of TC4 samples irradiated by ICP at constant power input of 800 W with different passes: three passes (a), five passes (b) and ten passes (c).

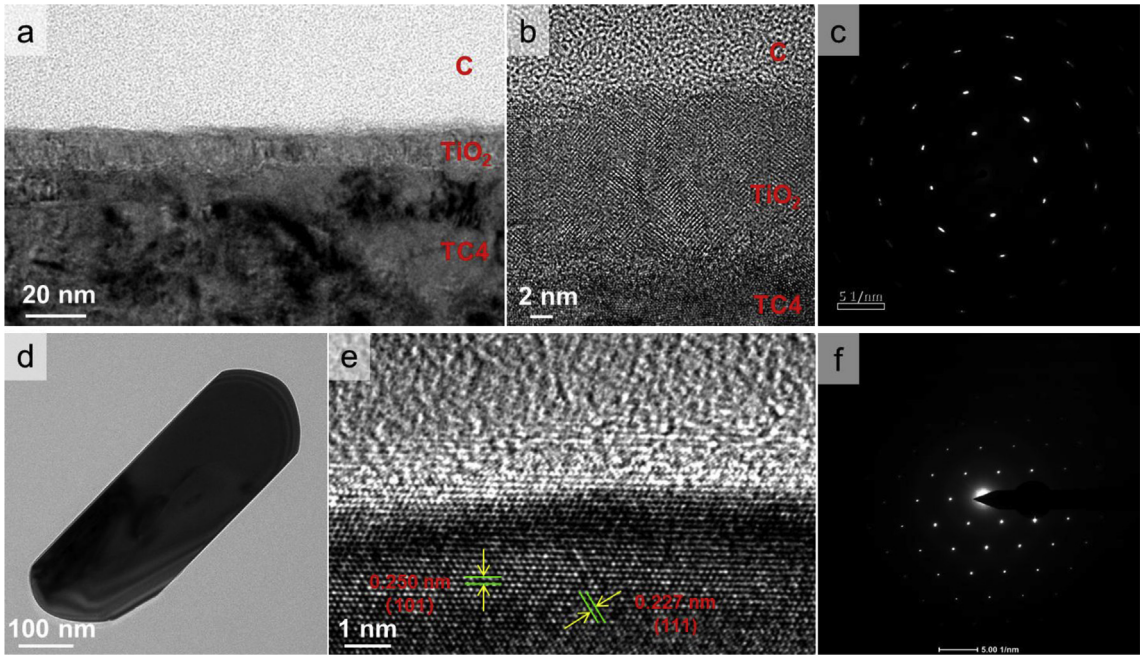

Fig. 7. TEM results and corresponding SAED patterns of TC4/TiO_2 and TiO_2 nanorods. (a) is a cross-sectional view of the treated TC4 (400 W, one pass) in Fig. 4(c). (b) is the HRTEM of (a). (c) is the SAED pattern of TC4/TiO_2 in (a). (d) is a close-up view of a TiO_2 nanorod peeled off the TC4 (800 W, five passes) in Fig. 5(b). (e) is the HRTEM of (d). (f) is the SAED pattern of the TiO_2 nanorod in (d).

Furthermore, we also investigated the growth of TiO_2 nanorods on TC4 samples after anodizing. The parameters of anodizing were described in Section 2.1. Fig. 10(a) and (a-1) show the surface morphology of anodized TC4, on which a layer of TiO_2 nanofilm was formed. The anodized sample was then irradiated by the ICP to induce the growth of TiO_2 nanorods. Unfortunately, similar to that of polished TA2, only short-length nano-bulges were obtained, as shown in Fig. 10(b) and (b-1). In addition, after the formation of TiO_2 nanofilm on TC4 substrate by anodizing, the blocking effect of β phase on thermal transmission disappeared, thus preventing local enhancement in temperature. Hence, TiO_2 nano-bulges could not grow into TiO_2 nanorods.

3.4. Characterization of optical, electrochemical, and hydrophilic properties of TiO_2 nanorods

TiO_2 is a wide band gap transparent semiconductor oxide with many outstanding properties [3]. In this paper, UV–Vis absorption

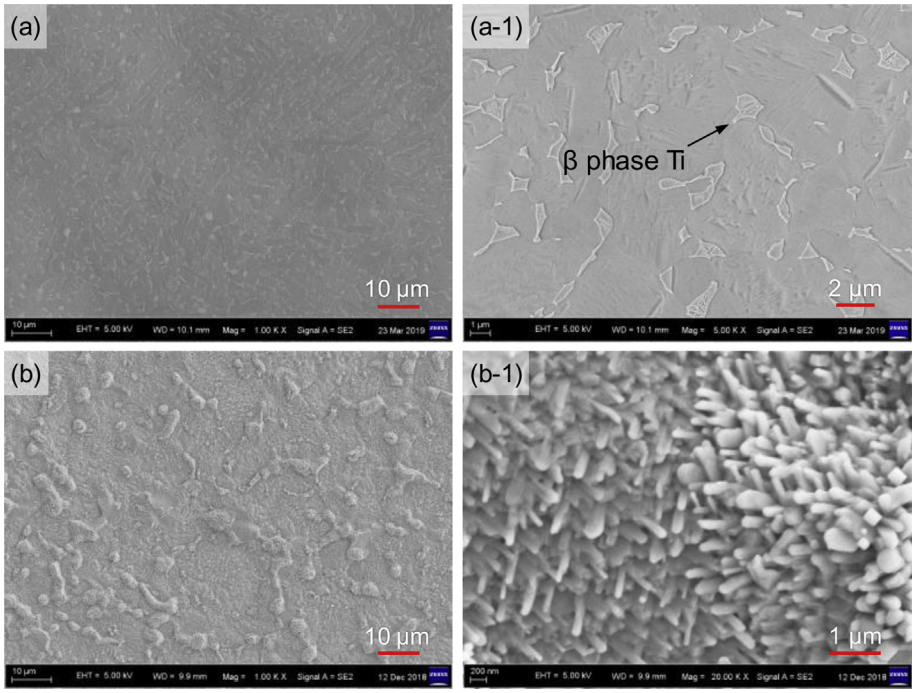

Fig. 8. Images of the TC4 samples processed by ECP and ICP (P_{in} = 800 W, one pass) successively. (a) SEM image of polished TC4 by ECP. (a-1) High magnification SEM image of (a). (b) SEM image of TC4 in (a) after irradiated by ICP. (b-1) High magnification SEM image of (b).

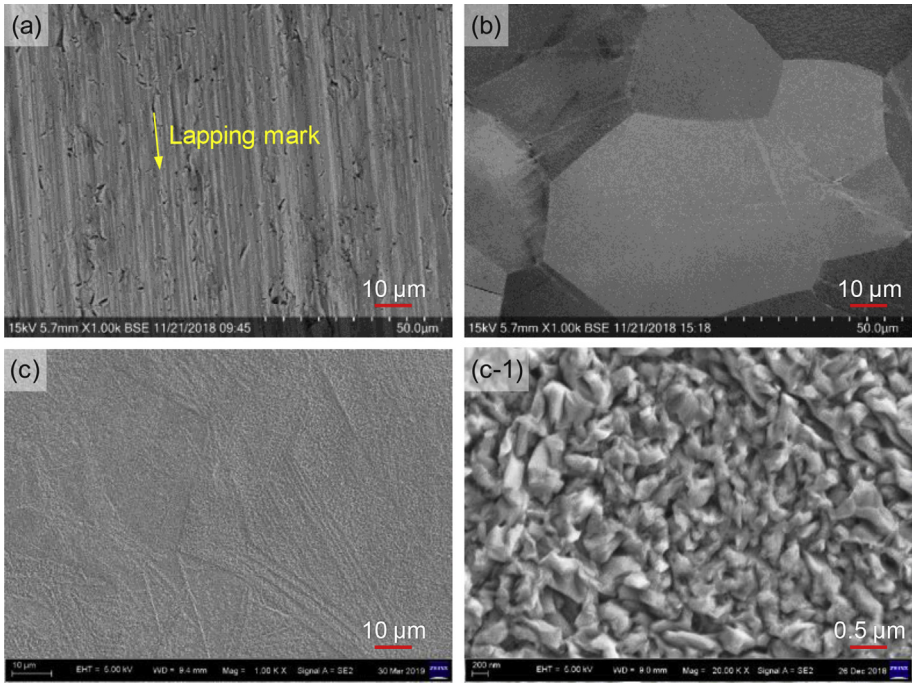

Fig. 9. Images of the TA2 sample processed by lapping, ECP and ICP (P_{in} = 800 W, one pass) successively. (a) SEM image of TA2 after lapping. (b) SEM image of TA2 in (a) after ECP. (c) SEM image of TA2 in (b) after irradiated by ICP. (c-1) High magnification SEM image of (c).

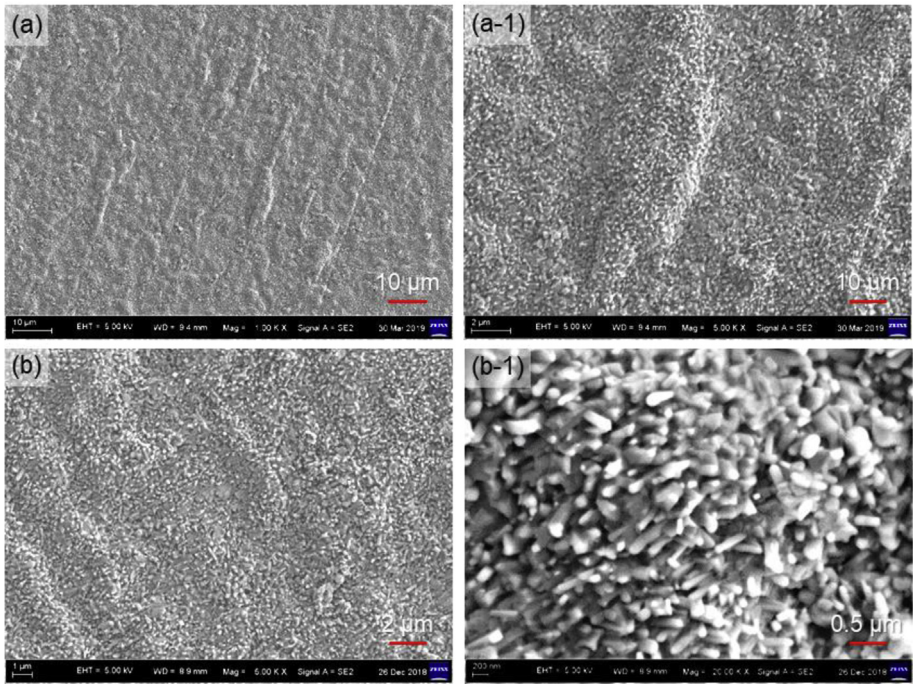

Fig. 10. Images of the TC4 sample processed by anodizing and ICP (P_{in} = 800 W, one pass) successively. (a) SEM image of TC4 after anodizing. (a-1) High magnification SEM image of (a). (b) SEM image of TC4 in (a) after irradiated by ICP. (b-1) High magnification SEM image of (b).

spectrum, cyclic voltammetry curve, and water contact angle (WCA) of TiO_2 nanorods were measured to characterize the optical, electrochemical, and hydrophilic properties, respectively.

The optical band gap (E_g) of TiO_2 nanofilm can be estimated by extrapolating tangent method using Tauc formula, which is conducive to understand the photoelectric property of materials [28]. The Tauc formula relating absorption coefficient α and E_g of semiconductor material is as follows:

$$\alpha h\nu = A(h\nu - E_g)^n,$$

where h is the Plank's constant; ν is the frequency of light; A is a constant factor determined by the transition probability; and n is a number associated with the type of transition (e.g. n = 1/2, 2, 3/2, or 3 for allowed direct, allowed indirect, forbidden direct and forbidden indirect electronic transitions, respectively) [28]. If α satisfies the following equation:

$$\alpha = \frac{2.303A}{d},$$

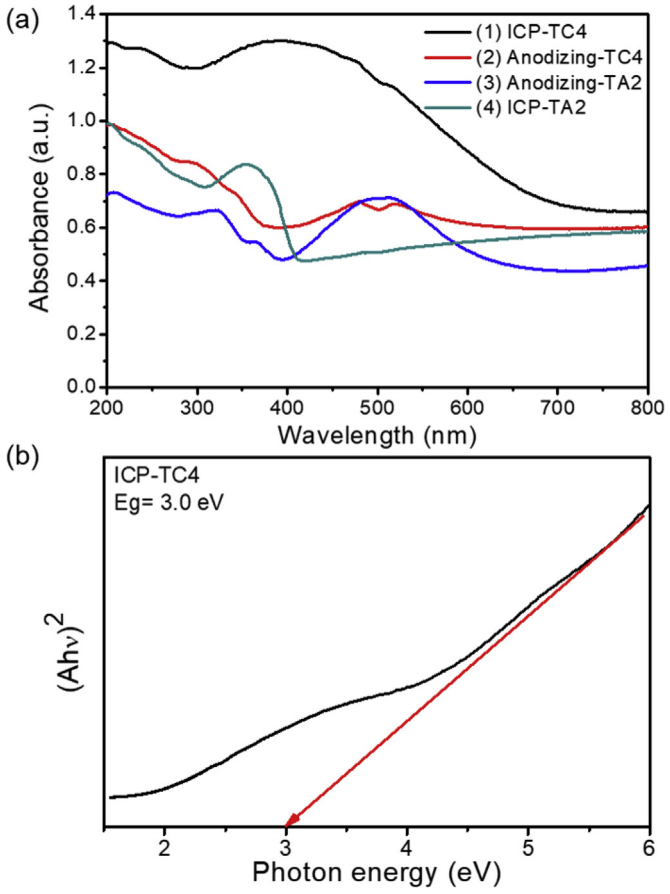

Fig. 11. Characterization results of optical property of TiO_2. (a) UV–Vis absorption spectrum of TiO_2 synthesized on TC4 and TA2 substrate by ICP treatment and anodizing, respectively. (b) Relation between $(Ahv)^2$ and the photon energy (eV) of TiO_2 nanorods synthesized on TC4 substrate by ICP treatment (P_{in} = 800 W, one pass).

where d is the thickness of TiO_2 nanofilm. Then, we can get

$$\left(\frac{2.303}{d}\right)^2 \times (Ahv)^2 = A(hv - E_g).$$

thus, based on the above equation, the value of E_g can be determined.

Fig. 11(a) shows the UV–Vis absorption spectrum of TiO_2 synthesized by different methods such as ICP treated TC4 and TA2 (P_{in} = 800 W, one pass), and anodizing treated TC4 and TA2. The relevant experimental details were mentioned in Section 2.1. Although, all samples present an apparent absorption enhancement phenomenon, ICP-TC4 sample, however, shows the strongest light absorption intensity as compared with other samples (anodizing-TC4, anodizing-TA2 and ICP-TA2) having relatively lower but different absorption intensity in the range of 200 to 800 nm. This significantly large absorbance arises due to the good morphology and the high-crystallinity of TiO_2, which can only be achieved for TiO_2 nanorods synthesized on TC4 substrate by ICP treatment. In visible light band, a large amount of oxygen vacancies can cause defect absorption, and neither mild anodizing for TC4 and TA2 nor violent ICP processing for TA2 would contribute to the growth of well-crystallized TiO_2 nanorods. Additionally, according to Fig. 11(b), the band gap of TiO_2 on ICP-TC4 sample estimated by extrapolation is about 2.9–3.0 eV, which is in excellent agreement with the band gap of rutile (3.0 eV) reported in literatures [14,29]. Thus, combining XRD analysis in Section 3.2 and above results, it is concluded that rutile phase TiO_2 nanorods with an absorption enhancement of UV–Vis light can be efficiently synthesized on TC4 substrate by ICP treatment under the condition of P_{in} = 800 W and one pass.

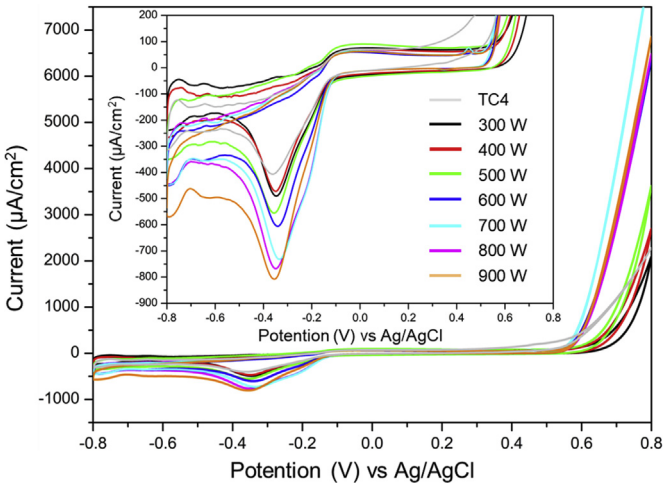

Fig. 12. CV curves of TiO_2 synthesized on TC4 substrate by ICP (P_{in} = 300–900 W, one pass) over the voltage range of −0.8 to 0.8 V.

The electrochemical behavior of as-received TC4 and treated TC4 samples by ICP irradiation under different conditions was studied by cyclic voltammetry (CV) at a scan speed 0.05 mV/s in a potential window from −0.8 to 0.8 V (vs Ag/AgCl), as depicted in Fig. 12. Notably, with the increase of P_{in}, the intensity of reduction peak of TiO_2 would become stronger and stronger, which indicates that TiO_2 nanorods formed at high P_{in} possess better electrochemical property. In addition, the CV curves hardly changed after five cycles of scanning. Thus, it can be said that the electrochemical property of TiO_2 nanorod is relatively stable.

The hydrophilic property of TiO_2 nanorods were determined by a contact angle instrument, and the relevant test details were illustrated in Section 2.4. The WCA between the deionized water droplet and the sample surface is inversely proportional to the hydrophilicity of the sample, which means that smaller WCA is a measure of the better hydrophilicity of the sample. Generally, a surface with WCA less than 15° would present high fluidity feature, while the surfaces with WCA less than 10° or 7° have the function of self-cleaning or anti-fogging [30]. In this study, the WCA of as-received TC4 was 53.4°, which dropped dramatically after irradiated by ICP at different P_{in} for one pass, as shown in Fig. 13(a). Even for P_{in} = 300 W, the corresponding WCA dropped to about half of the initial value. However, no significant changes of WCA can be observed with increasing P_{in} from 500 to 900 W. Theoretically, infect TiO_2 being a photosensitive n-type semiconductor oxide would generate oxygen vacancies and electrons, when exposed to UV light, consequently promoting the conversion of Ti^{4+} into Ti^{3+} [2]. Thus, the addition of water molecules on its surface would occupy oxygen vacancies to form hydroxyl groups. Hence, the interaction between TiO_2 surface and polar water molecules would become stronger, eventually forming the hydrophilic microcells. Similarly, ICP being a source of UV light immediately generates oxygen vacancies on the surface of TiO_2 even at P_{in} = 300 or 400 W. The oxygen vacancies play a decisive role in the value of WCA, thus at P_{in} = 500 W with surface area being unchanged, the WCA reduced to ~10° and the oxygen vacancies became almost saturated. Although the increasing P_{in} (600–900 W) did not significantly improve the oxygen vacancies, large surface area of TiO_2 nanorods further promoted the reduction of WCA slowly, as shown in Fig. 13(a). Therefore, a sample with WCA less than 5° exhibiting super hydrophilic property and excellent anti-fog function was synthesized at P_{in} = 900 W for one pass. However, Plasma irradiation at P_{in} = 900 W would easily cause the TiO_2 nanorod layer on the TC4 substrate to crack or even fall off.

Fig. 13(b) shows the variation in WCA of ICP (P_{in} = 800 W, one pass) treated TC4 as a function of the time. It seems that the value of WCA increased continuously and the hydrophilicity kept decreasing at

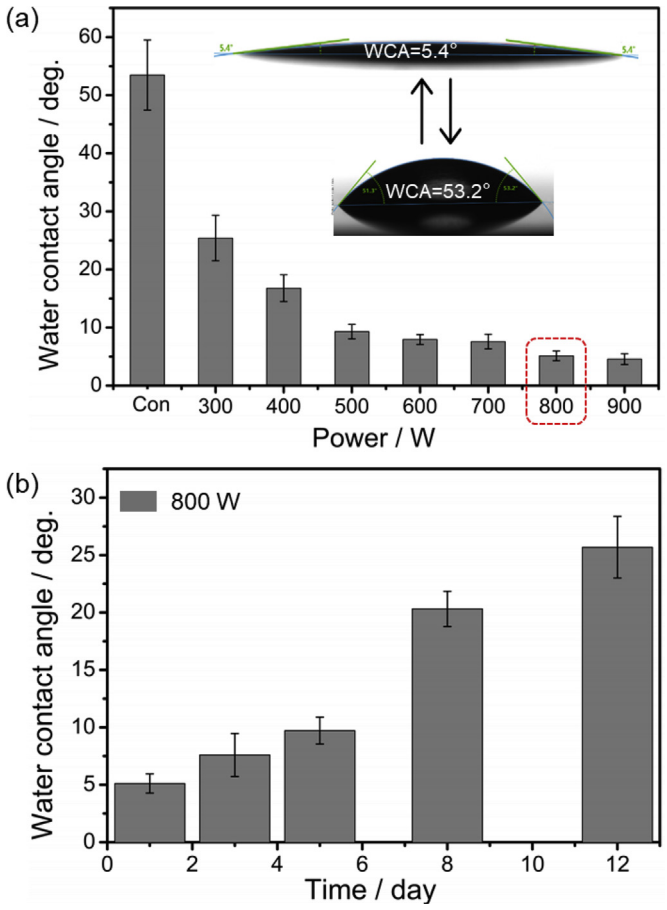

Fig. 13. Characterization results of hydrophilic property of TiO_2. (a) WCA of as-received TC4 and ICP treated TC4 at P_{in} = 300–900 W for one pass. The two insets show the WCA of as-received TC4 (53.2°) and ICP treated TC4 (5.4°) at P_{in} = 800 W, respectively. (b) WCA variation as function of time for ICP treated TC4 at P_{in} = 800 W for one pass.

snail's pace. After exposure to ambient air for three days, the WCA of the sample did not change much from its final value at the end of ICP irradiation experiments. Even after twelve days, the WCA was still not more than 28°. This trend of gradually increasing WCA can be attributed to the loss of oxygen vacancies and the accumulation of impurities such as dust on the sample surface. After ICP irradiation, the oxygen vacancies on the sample surface start capturing electrons or active hydroxyl groups and keep losing their activity. Moreover, oxygen vacancies occupied by the hydroxyl groups that are formed due to the absorbance of water molecules from ambient air, are once again gradually occupied by the oxygen. Ultimately, it can be concluded that TiO_2 nanorods synthesized by ICP on TC4 substrate exhibit excellent hydrophilicity with extended durability, as compared with the reports in different studies [11,31,32].

4. Conclusions

In this paper, rutile TiO_2 nanorods with excellent optical, electrochemical, and hydrophilic properties were synthesized on TC4 substrate by ICP irradiation, and the corresponding growth mechanism was studied. To summarize, the following conclusions can be drawn from the experimental results:

(1) Based on the strong chemical reactivity and high temperature characteristic of ICP at relatively high P_{in}, TiO_2 nanorods can be synthesized directly and rapidly on TC4 substrate.
(2) With ICP irradiation at constant P_{in}, longitudinal growth of TiO_2 nanorods is facilitated by prolonging the plasma processing time, which is suitable to grow different sizes of TiO_2 nanorods by controlling the processing time.
(3) The composition of substrate determines the quality of TiO_2 nanorods synthesized by ICP irradiation. Specifically, β phase Ti, which could suppress the thermal transmission between grains, is an important factor in the formation of TiO_2 nanorods. Compared with the polished TA2 by ECP and the oxidized TC4 by anodizing, TiO_2 nanorods with improved morphology can only grow on the polished TC4 by ECP due to the existing β phase Ti.
(4) TiO_2 nanorods synthesized on TC4 substrate by ICP irradiation show excellent optical, electrochemical, and hydrophilic properties, thus having potential applications in many fields, for example, photocatalysis and self-cleaning materials.

Declaration of interests

The authors declare that they have no known competing financial interests or personal relationships that could have appeared to influence the work reported in this paper.

Acknowledgements

This work was financially supported by the research fund for Basic Research of Free Exploration (JCYJ20180302174311087) and the research fund for International Cooperation (GJHZ20180928155412525 and GJHZ20180411143558312) from the Science and Technology Innovation Committee of Shenzhen Municipality, Shenzhen, China. This work was also supported by the Pico Center at SUSTech, Shenzhen, China.

References

[1] O. Carp, C.L. Huisman, A. Reller, Photoinduced reactivity of titanium dioxide, Prog. Solid State Chem. 32 (2004) 33–177.
[2] Y. Zhang, Z. Xing, X. Liu, Z. Li, X. Wu, J. Jiang, M. Li, Q. Zhu, W. Zhou, Ti^{3+} self-doped blue TiO_2(B) single-crystalline nanorods for efficient solar-driven photocatalytic performance, ACS Appl. Mater. Interfaces 8 (2016) 26851–26859.
[3] S. Kment, F. Riboni, S. Pausova, L. Wang, L. Wang, H. Han, Z. Hubicka, J. Krysa, P. Schmuki, R. Zboril, Photoanodes based on TiO_2 and α-Fe_2O_3 for solar water splitting - superior role of 1D nanoarchitectures and of combined heterostructures, Chem. Soc. Rev. 46 (2017) 3716–3769.
[4] H.S. Kim, J.W. Lee, N. Yantara, P.P. Boix, S.A. Kulkarni, S. Mhaisalkar, M. Gratzel, N.G. Park, High efficiency solid-state sensitized solar cell-based on submicrometer rutile TiO_2 nanorod and $CH_3NH_3PbI_3$ perovskite sensitizer, Nano Lett. 13 (2013) 2412–2417.
[5] K. Liu, L. Jiang, Bio-inspired self-cleaning surfaces, Annu. Rev. Mater. Res. 42 (2012) 231–263.
[6] A.M. Ruiz, G. Sakai, A. Cornet, K. Shimanoe, J.R. Morante, N. Yamazoe, Microstructure control of thermally stable TiO_2 obtained by hydrothermal process for gas sensors, Sens. Actuators B Chem. 103 (2004) 312–317.
[7] M. Wei, Z.-m. Qi, M. Ichihara, I. Honma, H. Zhou, Ultralong single-crystal TiO_2-B nanowires: synthesis and electrochemical measurements, Chem. Phys. Lett. 424 (2006) 316–320.
[8] T.R. Gordon, M. Cargnello, T. Paik, F. Mangolini, R.T. Weber, P. Fornasiero, C.B. Murray, Nonaqueous synthesis of TiO_2 nanocrystals using TiF_4 to engineer morphology, oxygen vacancy concentration, and photocatalytic activity, J. Am. Chem. Soc. 134 (2012) 6751–6761.
[9] N. Rahimi, R.A. Pax, E.M. Gray, Review of functional titanium oxides. I: TiO_2 and its modifications, Prog. Solid State Chem. 44 (2016) 86–105.
[10] K. Nakata, A. Fujishima, TiO_2 photocatalysis: design and applications, J. Photochem. Photobiol. C Photochem. Rev. 13 (2012) 169–189.
[11] X. Peng, A. Chen, Aligned TiO_2 nanorod arrays synthesized by oxidizing titanium with acetone, J. Mater. Chem. 14 (2004).
[12] J. Wang, D.N. Tafen, J.P. Lewis, Z. Hong, A. Manivannan, M. Zhi, M. Li, N. Wu, Origin of photocatalytic activity of nitrogen-doped TiO_2 nanobelts, J. Am. Chem. Soc. 131 (2009) 12290–12297.
[13] Y. Xu, W. Wen, J.M. Wu, Titania nanowires functionalized polyester fabrics with enhanced photocatalytic and antibacterial performances, J. Hazard Mater. 343 (2018) 285–297.
[14] X. Zhou, N. Liu, P. Schmuki, Photocatalysis with TiO_2 nanotubes: “colorful” reactivity and designing site-specific photocatalytic centers into TiO_2 nanotubes, ACS Catal. 7 (2017) 3210–3235.
[15] A. Fujishima, X. Zhang, D. Tryk, TiO_2 photocatalysis and related surface phenomena, Surf. Sci. Rep. 63 (2008) 515–582.

[16] W. Wen, J.M. Wu, Y.Z. Jiang, S.L. Yu, J.Q. Bai, M.H. Cao, J. Cui, Anatase TiO_2 ultrathin nanobelts derived from room-temperature-synthesized titanates for fast and safe lithium storage, Sci. Rep. 5 (2015) 11804.
[17] S. Kment, P. Kluson, H. Zabova, A. Churpita, M. Chichina, M. Cada, I. Gregora, J. Krysa, Z. Hubicka, Atmospheric pressure barrier torch discharge and its optimization for flexible deposition of TiO_2 thin coatings on various surfaces, Surf. Coat. Technol. 204 (2009) 667–675.
[18] T. Ichiki, R. Taura, Y. Horiike, Localized and ultrahigh-rate etching of silicon wafers using atmospheric-pressure microplasma jets, J. Appl. Phys. 95 (2004) 35–39.
[19] S.I. Hosseini, N. Farrokhi, K. Shokri, M.R. Khani, B. Shokri, Cold low pressure O_2 plasma treatment of Crocus sativus: an efficient way to eliminate toxicogenic fungi with minor effect on molecular and cellular properties of saffron, Food Chem. 257 (2018) 310–315.
[20] Y. Zhang, R. Li, Y. Zhang, D. Liu, H. Deng, Indiscriminate revelation of dislocations in single crystal SiC by inductively coupled plasma etching, J. Eur. Ceram. Soc. 39 (2019) 2831–2838.
[21] J. Zhang, M. Li, Z. Feng, J. Chen, C. Li, UV Raman spectroscopic study on TiO_2. I. Phase transformation at the surface and in the bulk, J. Phys. Chem. B 110 (2006) 927–935.
[22] Q. Xiang, D. Lang, T. Shen, F. Liu, Graphene-modified nanosized Ag_3PO_4 photocatalysts for enhanced visible-light photocatalytic activity and stability, Appl. Catal. B Environ. 162 (2015) 196–203.
[23] A. Monshi, M.R. Foroughi, M.R. Monshi, Modified scherrer equation to estimate more accurately nano-crystallite size using XRD, World J. Nano Sci. Eng. 2 (2012) 154–160.
[24] A.R. Shankar, N.S. Karthiselva, U.K. Mudali, Thermal oxidation of titanium to improve corrosion resistance in boiling nitric acid medium, Surf. Coat. Technol. 235 (2013) 45–53.
[25] M.E. Straumanis, T. Ejima, W.J. James, The TiO_2 phase explored by the lattice constant and density method, Acta Crystallogr. 14 (1961) 493–497.
[26] G. Liu, J.C. Yu, G.Q. Lu, H.M. Cheng, Crystal facet engineering of semiconductor photocatalysts: motivations, advances and unique properties, Chem. Commun. 47 (2011) 6763–6783.
[27] B. Liu, E.S. Aydil, Growth of oriented single-crystalline rutile TiO_2 nanorods on transparent conducting substrates for dye-sensitized solar cells, J. Am. Chem. Soc. 131 (2009) 3985–3990.
[28] V.M. Huxter, T. Mirkovic, P.S. Nair, G.D. Scholes, Demonstration of bulk semiconductor optical properties in processable Ag_2S and EuS nanocrystalline systems, Adv. Mater. 20 (2008) 2439–2443.
[29] F. Su, T. Wang, R. Lv, J. Zhang, P. Zhang, J. Lu, J. Gong, Dendritic Au/TiO_2 nanorod arrays for visible-light driven photoelectrochemical water splitting, Nanoscale 5 (2013) 9001–9009.
[30] S. Banerjee, D.D. Dionysiou, S.C. Pillai, Self-cleaning applications of TiO_2 by photo-induced hydrophilicity and photocatalysis, Appl. Catal. B Environ. 176–177 (2015) 396–428.
[31] X. Peng, J. Wang, D.F. Thomas, A. Chen, Tunable growth of TiO_2 nanostructures on Ti substrates, Nanotechnology 16 (2005) 2389–2395.
[32] Q. Gao, X. Wu, Y. Fan, X. Zhou, Fabrication of hierarchically structured rutile TiO_2 nanorods on mica particles and their superhydrophilic coating without UV irridiation, Appl. Surf. Sci. 289 (2014) 281–288.